ADVANCED FUNCTIONAL MATERIALS
www.afm-journal.de

Designing Reflective Hybrid Counter Electrode for Fiber Dye-Sensitized Solar Cell with Record Efficiency

*Zhengfeng Zhu, Zhengmeng Lin, Yu Gu, Jiatian Song, Xinyue Kang, Hongyu Jiang, and Huisheng Peng**

Fiber solar cells can be woven into textiles to effectively supply electricity for wearables and have attracted increasing interests in the past decade. However, achieving high power conversion efficiencies in real-world applications remains a significant challenge for power supply textiles. Here a unique hybrid counter electrode made from metal current collector fiber with high electrical conductivity, aligned carbon nanotube sheet with high electrocatalytic property, and porous titanium dioxide/poly(vinylidene fluoride-*co*-hexafluoropropylene) film with high light reflectance is designed. For the resulting fiber dye-sensitized solar cell, a rapid charge collection and transport are achieved, and the unique advantage of absorbing light from all directions is effectively realized, producing a record power conversion efficiency of 12.52%. The power conversion efficiency varies below 10% after bending, twisting, or pressing for 1000 cycles. These fiber dye-sensitized solar cells are further integrated with fiber batteries as power systems for a smart bracelet, demonstrating the effective power solution for wearables.

1. Introduction

In the past decade, wearables have been booming in many important fields, such as communication, information interaction, motion monitoring, medical care, and personal health management.[1–4] It is critical while challenging to find effective and endurable power supplies for current wearables and especially emerging smart electronic textiles.[5–7] To this end, fiber solar cells with advantages of flexibility and light weight have been widely explored to produce textiles as promising power systems.[8–12] Although extensive efforts in the synthesis of novel functional materials,[13–15] optimization of device structures,[16] and design of stable interfaces between active layers and substrates,[17] the present fiber solar cells show relatively low power conversion efficiencies (PCEs) due to the difficulty of high-quality device fabrication on curved fibers, which has severely limited their further development, particularly for real applications in wearables.[18–20] Another possible solution to this bottleneck problem lies in the strategy to take the unique advantage of fiber solar cells in comparison to their planar counterparts, i.e., effectively absorbing light from 360° directions. Sufficient utilization of the active layer covered around fiber for more efficient light harvesting is a promising way to enhance the photovoltaic performance of fiber solar cells. Despite the urgent demand, unfortunately, it remains unavailable.

In this work, we designed a unique hybrid counter electrode made from metal current collector fiber with high electrical conductivity, aligned carbon nanotube (CNT) sheet with high electrocatalytic property,[21–24] and porous titanium dioxide/poly(vinylidene fluoride-*co*-hexafluoropropylene) [TiO_2/P(VDF-HFP)] film with high light reflectance for fiber dye-sensitized solar cells (FDSSCs). The inner CNT sheet closely attached to highly conductive metal fiber promoted charge collection and transport, while the outer porous film composed of TiO_2 nanoparticles uniformly dispersed in P(VDF-HFP) realized strong diffuse reflection at wavelengths of 400–750 nm with an average reflectance as high as 93.37%, and the consecutive pores established stable pathways for ion diffusion within the electrolyte, ensuring consistent and reliable ion transport. For the resulting FDSSC, the photoanode effectively took advantage of fiber shape to extensively harvest light reflected from the hybrid counter electrode, remarkably enhancing photocurrent to produce a record PCE of 12.52%. These efficient FDSSCs were further integrated with fiber batteries into textiles and successfully powered a smart bracelet, demonstrating an effective power solution for wearables.

2. Results and Discussion

Figure 1a depicts the designed structure of FDSSC with the photoanode composed of aligned TiO_2 nanotubes grown on a Ti wire (Figure S1, Supporting Information) and the counter electrode

Z. Zhu, Z. Lin, J. Song, X. Kang, H. Jiang, H. Peng
State Key Laboratory of Molecular Engineering of Polymers
Department of Macromolecular Science, Institute of Fiber Materials and Devices, and Laboratory of Advanced Materials
Fudan University
Shanghai 200438, China
E-mail: penghs@fudan.edu.cn

Y. Gu
Key Laboratory of Advanced Display Materials and Devices
Ministry of Industry and Information Technology
Institute of Optoelectronics and Nanomaterials, College of Material Science and Engineering
Nanjing University of Science and Technology
Nanjing 210094, China

The ORCID identification number(s) for the author(s) of this article can be found under https://doi.org/10.1002/adfm.202306742

DOI: 10.1002/adfm.202306742

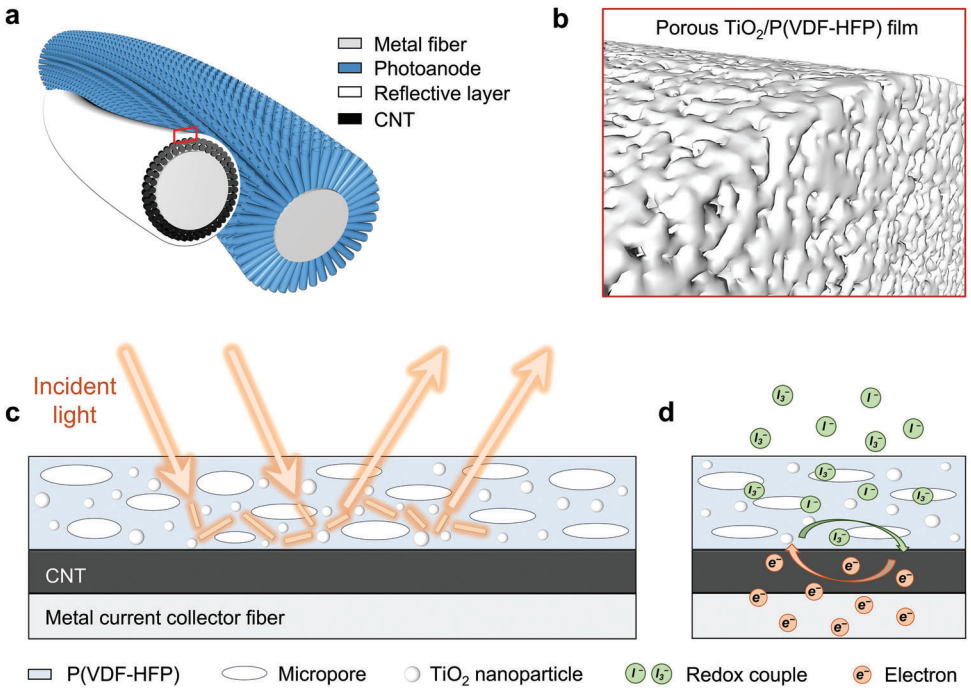

Figure 1. Schematic diagram of FDSSC with the hybrid counter electrode. a) Diagram illustrating the device structure of FDSSC with the photoanode made from a radically aligned TiO_2 nanotube array and the counter electrode composed of a metal fiber, an aligned CNT sheet, and a reflective layer. b) Diagram of the structure of reflective layer marked in (a), composed of porous TiO_2/P(VDF-HFP) film. c) Sketch map showing the propagation path of incident light in the reflective layer. The incident light is refracted and scattered by TiO_2 nanoparticles in the reflective layer, then diffuses out. d) Schematics showing that the porous structure provides channels for rapid migration and reaction of redox mediators throughout the whole system.

consisting of a metal current collector fiber, aligned CNT sheet, and reflective layer made from porous TiO_2/P(VDF-HFP) film (Figure 1b). The incident light across the reflective layer would experience multiple scatterings and refractions due to the appropriate sizes of TiO_2 nanoparticles and their high refractive index ratio with P(VDF-HFP),[25–28] which finally propagates out of the film, showing diffuse reflections (Figure 1c). Moreover, the porous structure provides successive channels for rapid diffusion of redox mediators between electrodes and the metal current collector would promote efficient charge collection and transport in FDSSC (Figure 1d).

The hybrid counter electrode can be continuously prepared and is schematically illustrated in **Figure 2**a. In brief, the aligned CNT sheet was synthesized by floating catalyst chemical vapor deposition method (Figure S2, Supporting Information). Subsequently, the CNT sheet was tightly wrapped around a metal fiber and coated with a slurry of TiO_2/P(VDF-HFP). The coated structure underwent a nonsolvent exchange process[29–31] and drying, after which it was wound continuously on reels (Figure 2b). The obtained hybrid fiber exhibited homogeneous diameter distribution with a small variation of less than 2% (Figure 2c). In the resulting counter electrode, aligned CNT sheet was closely attached to a metal fiber made from aligned stainless-steel wires twisted around a nylon fiber (Figure 2d). The formed CNT/metal fiber with compact and stable interfaces achieved much lower electrical resistance and electrochemical impedance in contrast with twisted CNT fiber typically investigated before, causing more efficient charge collection and transport to improve photovoltaic performance of FDSSCs (Figure S3, Supporting Information).

The suitable viscosity of highly dispersed TiO_2/P(VDF-HFP) slurry is critical for the formation of high-quality film on curved fiber by dip-coating mothed, as low viscosity could not overcome the surface tension of slurry and cause aggregations like beads (Figure S4, Supporting Information). TiO_2 nanoparticle slurry is a typical nanofluid, and its viscosity could be effectively improved by increasing volume fraction of nanoparticles,[32–34] promoting uniform and smooth film formation on CNT/metal fiber (Figure 2e). In the produced TiO_2/P(VDF-HFP) film, TiO_2 nanoparticles were incorporated into the porous polymer matrix, and large amounts of pores distributed in the film with hundreds of nanometers constituted successive channels, beneficial for the rapid diffusion of redox mediators in electrolyte (Figure 2f,g). Furthermore, hybrid counter electrodes showed both high flexibility and mechanical strength (Figure S5, Supporting Information), which could ensure stable electrical connections of FDSSCs even under various complex deformations in the case of weaving applications.

To investigate optical properties of constructed porous TiO_2/P(VDF-HFP) film, we first used the finite difference time domain method to simulate optical field distribution inside the polymer film containing TiO_2 nanoparticles with irradiation under parallel light (**Figure 3**a). In the simulation, TiO_2 nanospheres with diameter of 300 nm were introduced into a polymer film with 15 μm thickness at random positions and their volume fraction was ≈50%. A plane wave source was placed above the structure and a power monitor perpendicular to the film surface was added to record the field profile. It clearly showed that the 500 nm light could not penetrate deeply into the

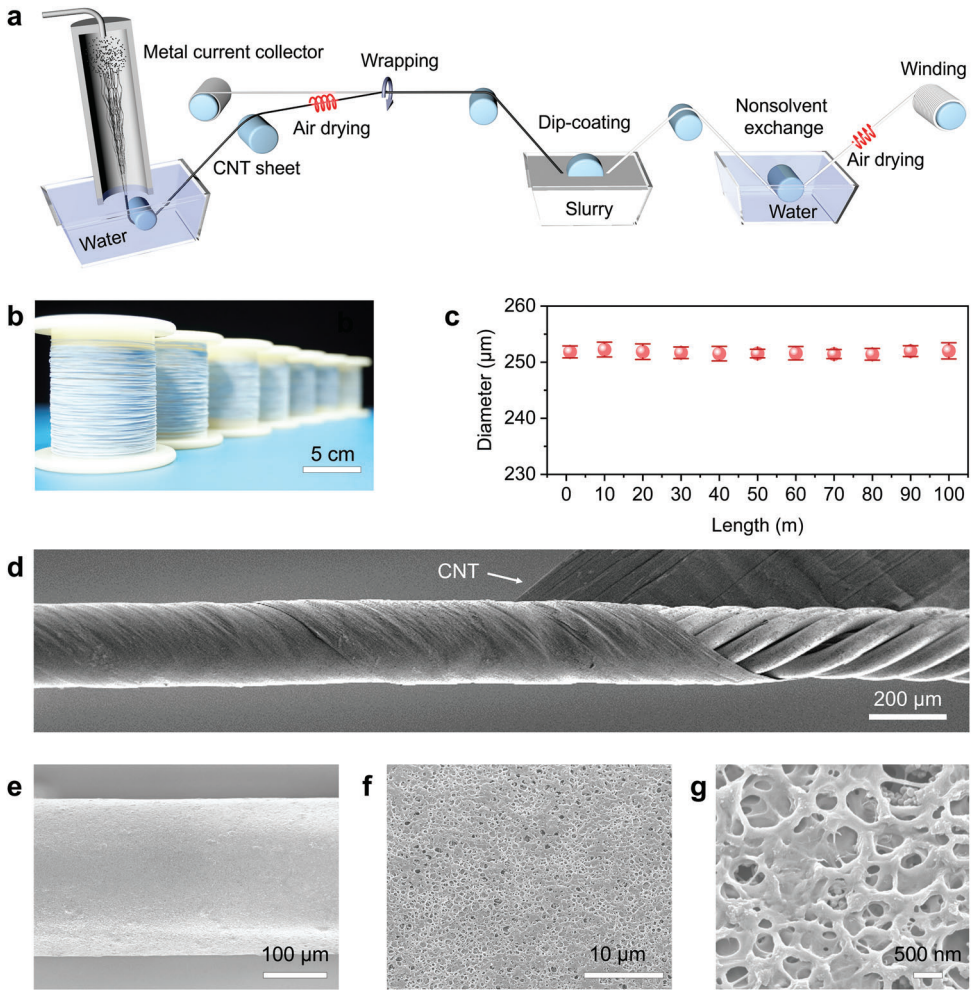

Figure 2. Preparation and structure of the hybrid counter electrode. a) Diagram showing the preparation flow of the hybrid counter electrode. After an aligned CNT sheet was synthesized by floating catalyst chemical vapor deposition and closely wrapped around a metal current collector, it was dip-coated with TiO_2/P(VDF-HFP) slurry, subsequently immersed in water to induce phase separation, then dried and winded on a reel. b) Photograph of several reels of the prepared hybrid counter electrode. c) Diameter distributions of the hybrid counter electrode in a length range of 100 m. Error bars, standard deviations of the results from three samples. d) SEM image of aligned CNT sheet closely attached to a highly flexible metal current collector that was prepared by twisting aligned stainless steel wires around an aramid fiber. e) SEM image of TiO_2/P(VDF-HFP) film. f,g) Magnified SEM images of TiO_2/P(VDF-HFP) film with a porous structure, where TiO_2 nanoparticles were embedded in P(VDF-HFP), at low and high magnifications, respectively.

polymer film due to multiple scatterings by the TiO_2 nanoparticles. Since we did not introduce any absorption into the system, one would expect a nearly 100% reflection for films thicker than 15 μm, confirming the effectivity of our designed reflective layer. Subsequently, a perfect diffuse reflection was assumed to illustrate the spatial optical field distribution after incident light reflected from a local planar unit and the whole cylindrical surface of fiber, respectively (Figure 3b,c), further demonstrating that the hybrid fiber counter electrode could effectively reflect incident light to the neighboring photoanode for enhanced light harvesting of FDSSC.

In the prepared reflective layer, TiO_2 nanoparticles with sizes at a range of 200–400 nm were incorporated into the P(VDF-HFP) for a wide scattering peak due to the collective effect of multiple Mie resonances of them,[35,36] thus producing strong light reflection at the wavelength range that precisely overlapped the absorption spectrum of N719 dye (Figure 3d). A high reflectance over 90% could be easily achieved by adjusting film thickness of reflective layer.[37] The FDSSC with reflective layer in counter electrode showed a marked increase in photocurrent (Figure S6, Supporting Information), demonstrating efficiently enhanced light harvesting of photoanode. An excessively thin film could not reflect sufficient amount of incident light, while an excessively thick layer increased the diffusion distances of redox mediators. Meanwhile, excessive amount of TiO_2 nanoparticles also caused obvious band-edge absorption, reducing reflectance at the wavelengths near 400–450 nm and causing light loss (Figure S7a, Supporting Information).[38,39] Therefore, with optimized thickness of ≈30 μm for the reflective layer in counter electrode, FDSSCs achieved a better photovoltaic performance than those with a thinner or a thicker reflective layer (Figure S7b and Table S1, Supporting Information).

Certainly, the porous structure of reflective layer was critical to the ion diffusion through the whole redox system, making the

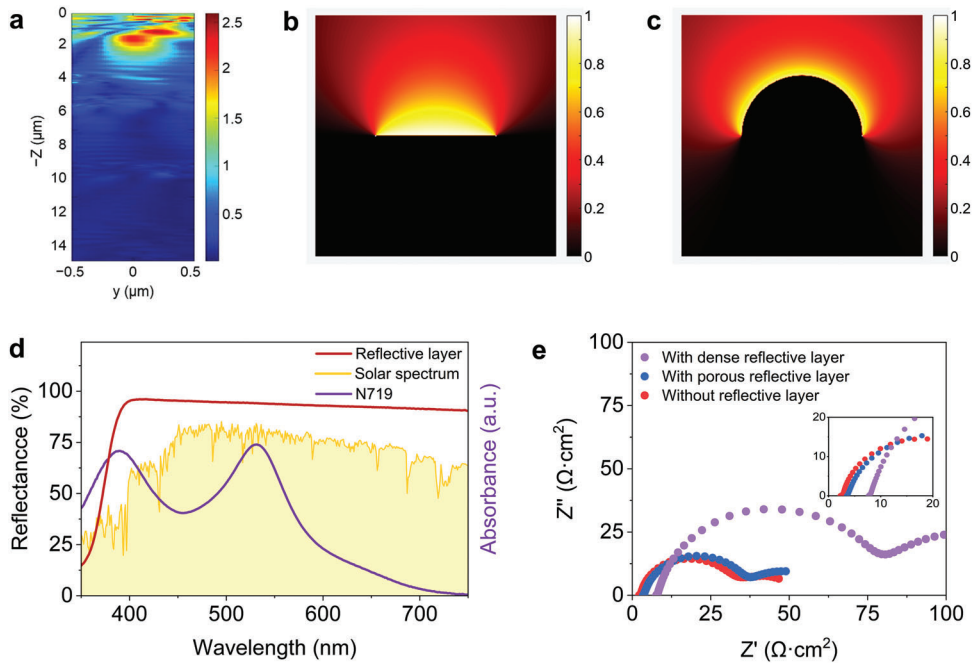

Figure 3. Properties of the hybrid counter electrode. a) Optical field distribution of the incident light in the porous TiO_2/P(VDF-HFP) film, simulated by finite-different time-domain method. The incident light suffered refraction and scattering, then diffused out the film. b,c) Simulated optical field distribution of diffused light from a planar and curved substrate with an ideal diffuse reflection mode, respectively. An infinitely long plane with a finite width is used for the planar surface and the cylindrical surface is also infinitely long with a diameter the same as the width of the planar surface. The plot shows the normalized radiation energy density. d) Absorbance and reflectance spectra of N719 dye and the reflective layer. e) Nyquist plots of symmetrical cells consisting of two identical electrodes measured at 0 V from 100 kHz to 0.01 Hz in an acetonitrile solution containing 6 mM I_2, 0.1 M LiI, 0.6 M 1,2-dimethyl-3-propylimidazolium iodide, and 1 M 4-tert-butylpyridine. Inset, enlarged view of Nyquist plots at high frequency. The corresponding Nernst diffusion impedances of CNT/metal fiber with a dense reflective layer, CNT/metal fiber with a porous reflective layer, and CNT/metal fiber without reflective layer were 73.24, 34.22, and 31.10 Ω cm^2, respectively.

hybrid counter electrode exhibit electrochemical properties equal to the inner CNT/metal fiber without obvious performance degeneration (Figure 3e). In contrast, the dense reflective layer without porous structure would seriously hinder the migration and then suppress reaction rates of redox mediators because of its much higher diffusion impedance (Figure 3e and Table S2, Supporting Information). Moreover, the dense film fully covered on the surface of CNT sheet greatly decreased the effective catalytic active areas in hybrid counter electrode,[40] severely degrading its catalytic properties (Figure S8a, Supporting Information). Therefore, the FDSSC with dense reflective layer showed terrible photovoltaic performance with a low PCE of 7.92% (Figure S8b, Supporting Information).

Finally, by designing highly reflective and highly conductive hybrid counter electrode, combined with fiber photoanode that could absorb incident light from 360° directions, the resulting FDSSC realized sufficient light harvesting and efficient charge transport. This improvement led to a remarkable 28.52% increase in power output compared to the FDSSC without reflective layer. It produces a record PCE of 12.52%, with short-circuit current (J_{SC}), open-circuit voltage (V_{OC}), and fill factor (FF) of 21.061 mA cm^{-2}, 0.777 V, and 0.765, respectively (**Figure 4**a and Table S3, Supporting Information). Compared to the dense reflective layer, the porous structure greatly reduced R_S in FDSSCs, only showing a slightly higher R_S value than that of the FDSSCs without reflective layer, which also accounted for their high PCEs (Figure S9, Supporting Information).

The PCE statistics from 50 FDSSCs with a narrow distribution demonstrated high repeatability and stability of the preparation technology, which could effectively meet future large-scale applications (Figure 4b). Our FDSSCs also exhibited high flexibility and mechanical stability against various deformations such as bending, twisting, and pressing (Figure 4c). Their PCEs maintained over 90% after undergoing 1000 cycles of different deformation modes. In addition, these FDSSCs could effectively work at increasing temperatures from −40 to 40 °C to satisfy various environments, showing stable power outputs with a PCE variation below 10% (Figure 4d). As the counter electrode partly coved on the photoanode in FDSSCs may influence light harvesting, we further explored their PCE dependency on incident light direction (Figure S10, Supporting Information). The PCEs of FDSSCs had been maintained by over 90% under the incident light from different directions at a broad range, which is important for practical applications.

The resulting FDSSCs were further integrated with fiber batteries into textiles as power systems, in which FDSSC modules can achieve desired output voltages and currents by connecting in series and parallel to match the charge voltage and current of fiber batteries, respectively (Figure 4e,f). The output voltages of photovoltaic modules exceeded the maximum voltage of batteries, while the output currents were controlled for appropriate

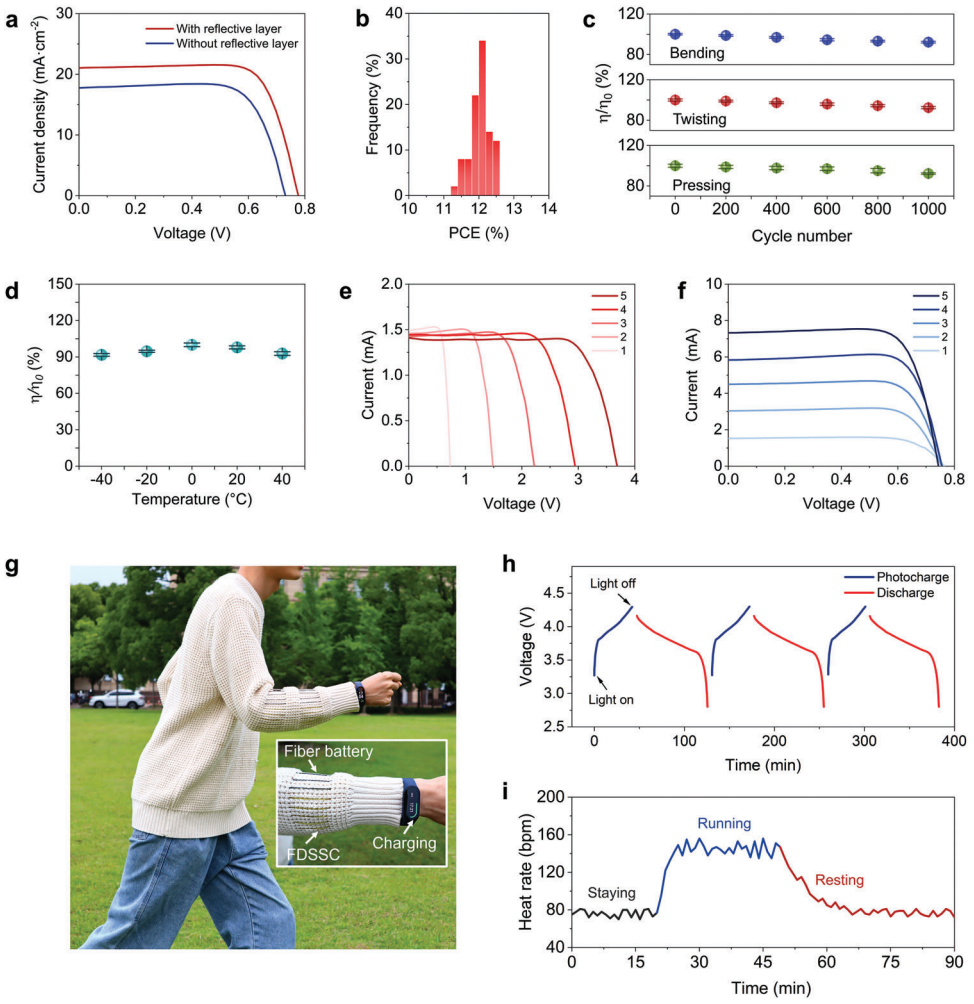

Figure 4. Photovoltaic properties of FDSSC. a) *J–V* curves of FDSSCs with and without reflective layer. b) PCE statistics of 50 FDSSCs. c) Mechanical stability of FDSSCs against bending, twisting, and pressing. Their performance variations were below 10% after 1000 cycles for each deformation mode. Error bars, standard deviations of the results from three samples. d) Stability of FDSSCs working under different temperatures. e) *I–V* curves of FDSSCs connected in series. f) *I–V* curves of FDSSCs connected in parallel. g) Photograph of a clothing integrated with FDSSCs and fiber lithium-ion batteries to power a smart bracelet. h) Photocharge/discharge curves of self-charging power system. A fiber lithium-ion battery with a capacity of 1.6 mAh was charged from 2.8 to 4.3 V by FDSSCs under simulated AM1.5G sunlight and then discharged to 2.8 V at 0.5 C rate. i) Real-time heart rate monitoring of the user in different states like staying, running, and resting.

charging rates according to the capacities of fiber batteries. The modules can charge fiber batteries for electricity storage and supply powers for wearables on demand (Figure 4g). In the power system, fiber lithium-ion battery was successfully charged from 2.8 to 4.3 V by FDSSCs under air mass 1.5 global (AM1.5G) sunlight (Figure 4h and Figure S11, Supporting Information), further powering a smart bracelet that has been widely used in our daily life and can record our real-time heart rates in different motion states like staying, running, and resting (Figure 4i). Our power supply textiles offer an effective solution for addressing the limited working duration typically imposed by built-in low-capacity batteries in wearables.

3. Conclusion

In summary, we had designed a unique porous hybrid counter electrode with high light reflectance. The resulting FDSSC could fully take advantage of fiber shape to harvest light from various directions for higher photocurrent. It produced remarkably enhanced photovoltaic performance with a PCE as high as 12.52%. These FDSSCs were further integrated with fiber batteries into textiles as power systems, demonstrating an effective power solution for wearables. Power supply textiles can be easily integrated with other fiber devices, opening up possibilities for future smart textile systems, which has the potential to revolutionize portable, flexible, and wearable electronic technologies in the future.

4. Experimental Section

Materials: Commercial titanium wire (metal basis: 99.9%, diameter: 150 µm), titanium oxide (anatase, metal basis: 99.8%, size: 200–400 nm, Aladdin), ammonium fluoride (metal basis: 99.99%, Aladdin), ethylene glycol (99.5%, Sinopharm), ethanol (99.7%, Sinopharm), tert-butyl alcohol (99%, Aladdin), *N*,*N*-dimethylformamide (99.5%,

Sinopharm), poly(vinylidene fluoride-*co*-hexafluoropropylene (pellets, Sigma-Aldrich), $LiClO_4$ (99.9%, Aladdin), acetonitrile (98%, Aladdin), iodine (99.8%, J&K), lithium iodide (anhydrous, 98.5%, J&K), 1,2-dimethyl-3-propylimidazolium iodide (98%, TOKYO CHEMICAL INDUSTRY CO., LTD.), 4-tert-butylpyridine (96%, Aladdin), acetone (99.5%, Sinopharm), isopropanol (99.7%, Sinopharm), N719 dye (high performance liquid chromatography: 90%, Aladdin), and heat-shrinking tubes (Zhongshan Wolida Electronic Material Co., Ltd.) were commercially available and used without further treatment unless otherwise mentioned.

Preparation of Fiber Photoanodes: TiO_2 nanotube array was prepared on a Ti wire by an anodization process. After Ti wire was cleaned with acetone, isopropanol, and deionized water, it was anodized at 60 V and 40 °C in an ethylene glycol solution containing 3.3 g L^{-1} NH_4F and 88 g L^{-1} H_2O for 6 h, then washed with deionized water. The anodized Ti wire was further annealed at 500 °C for 1 h with a heating rate of 8 °C min^{-1} starting from room temperature in a furnace. The dye solution of N719 was prepared by dissolving 0.3 mM N719 in tert-butyl alcohol/acetonitrile (1/1, v/v). The fiber photoanode was obtained after the cooled wire was immersed in the dye solution for 24 h.

Preparation of Fiber Hybrid Counter Electrodes: Aligned CNT sheet was prepared by floating catalyst chemical vapor deposition. The feed solution used ethanol as the carbon source mixed with 2.5 wt% ferrocene and 2 wt% thiophene as the composite catalyst. The solution was placed in a furnace at 1200 °C in a hydrogen and argon atmosphere with a flow rate of 0.2 mL min^{-1}. The synthesized CNT aerogels were removed from the furnace, densified through water, and dried in air to form continuous aligned CNT sheet. Then, the CNT sheet was closely attached onto a metal current collector made from several stainless-steel wires twisted around a nylon fiber at a specific angle to construct a core-sheath CNT/metal fiber. After P(VDF-HFP) and TiO_2 nanoparticles were dispersed in N,N-dimethylformamide (DMF) with a content of 24.44 wt% by stirring for 4 h at 70 °C, CNT/metal fiber was further dip-coated with TiO_2/P(VDF-HFP) slurry and soaked in water for 20 min, followed by air drying at 80 °C. Then, fiber hybrid counter electrode was obtained.

Fabrication of Fiber Dye-Sensitized Solar Cells: The electrolyte was prepared by dissolving 6 mM I_2, 0.1 M LiI, 0.6 M 1,2-dimethyl-3-propylimidazolium iodide, and 1 M 4-tert-butylpyridine in acetonitrile. To fabricate the FDSSC, a fiber photoanode twisted with a hybrid fiber counter electrode was encapsulated in a transparent tube with injected electrolyte.

Fabrication of Fiber Lithium-Ion Batteries: A fiber positive electrode was prepared by dip-coating a positive slurry (lithium cobalt oxide, super-P, polyvinylidene fluoride, *N*-methyl-2-pyrrolidone) on an Al wire (diameter of 200 µm). A fiber negative electrode was prepared by dip-coating a negative slurry (graphite, super-P, sodium carboxymethyl cellulose, butadiene styrene rubber, water) on a Cu wire (diameter of 200 µm). The two fiber electrodes were then wrapped with separator strips. The above electrodes were twisted and encapsulated in a tube with injected electrolyte.

Electrochemical Measurements: Electrochemical impedance spectra were measured by an electrochemical workstation (CHI 660E, Shanghai Chenhua). Cyclic voltammograms were obtained in acetonitrile solution containing 5 mM I^-, 0.5 mM I_2, and 0.05 M $LiClO_4$ at 50 mV s^{-1} with Ag/AgCl electrode, Pt, and as-prepared electrode as reference, counter, and working electrode, respectively.

Characterizations: *J–V* curves of FDSSCs were measured with a source meter (Keithley 2420) from 0.9 to −0.2 V with a dwell time of 50 ms under simulated AM1.5G sunlight. Absorption spectra of dye solutions and reflectance of the reflective layer were measured by a UV-visible spectrophotometer (Lambda 750, Perkin Elmer). Scanning electron microscopy (SEM) images were obtained by a field-emission scanning electron microscope (Zeiss Sigma, operated at 3 kV). The involved wearable sensor was a common commercial product and operated in strict accordance with the product instructions. The human experiments conformed to the regulation of the Animal and Human Experimentation Committee of Fudan University. A healthy subject from Fudan University had provided written informed consent before participating in the study.

Calculation of PCEs of FDSSCs: The effective area of FDSSC was represented by the projected area of the photoanode, calculated from its effective length and average diameter. The PCE of FDSSCs was calculated by the following equations

$$\mathrm{PCE} = \frac{I_{SC} \times V_{OC} \times \mathrm{FF}}{A \times P_{in}} \tag{1}$$

$$A = d \times l \tag{2}$$

where I_{SC} is the short-circuit current, P_{in} is the power density of incident light, A is the projected area of the photoanode, d is the average diameter of the photoanode, and l is the effective length of the photoanode.

FDTD Simulations: Finite difference time domain (FDTD) method was used to simulate the field distribution inside the polymer films containing TiO_2 nanoparticles. The polymer film showed thickness of 15 µm thick and the TiO_2 nanospheres with diameters of 300–400 nm were then incorporated into the system. The volume fraction was ≈46%. Spherical pores were also introduced to the composite film with volume fraction of ≈50%. A plane wave source was placed above and a power monitor perpendicular to the film surface was added to record the field profile. The refractive indexes of TiO_2, P(VDF-HFP), and air pore were taken as general values of 2.56, 1.4, and 1, respectively.

Simulation of Reflective Optical Fields: The incident light intensity is E_0 and a perfect diffuse reflection by an elementary surface dA results in an angular independent radiative intensity I_0. The two terms are related with the following equation

$$\int_{+2\pi} I_0 \cos\theta \mathrm{d}\Omega \mathrm{d}A = E_0 \, \mathrm{d}A \Rightarrow I_0 = \frac{E_0}{\pi} \tag{3}$$

Both surfaces are essentially treated as diffusely emitting surfaces. The radiation energy density of U_d at a certain point p in space is found by summing up all the contributions from the emitting surfaces.

$$U_d(\vec{r}) = \int_{4\pi} I(\vec{r}, \hat{s}) \, \mathrm{d}\Omega = \int I_0 \frac{\hat{n} \cdot (\vec{r}_A - \vec{r})}{|\vec{r}_A - \vec{r}|} \frac{\mathrm{d}A}{|\vec{r}_A - \vec{r}|^2}$$
$$= I_0 \int \frac{\hat{n} \cdot (\vec{r}_A - \vec{r})}{|\vec{r}_A - \vec{r}|^3} \mathrm{d}A \tag{4}$$

$\vec{r}$ is the position vector of the point of interest p in space, $\vec{r}$ is the position vector of the surface element dA, and $\hat{n}$ is the unit vector along the normal direction of dA. The integration is only taken when $\hat{n} \cdot (\vec{r}_A - \vec{r}) > 0$ is satisfied. An infinitely long plane with a finite width is used for the planar surface. The cylindrical surface is also infinitely long with a diameter the same as the width of the planar surface. The plot shows the normalized $U_d(\vec{r})$.

Statistical Analysis: The thickness of reflective layer is defined as half of the difference value between the average dimeters of fiber counter electrodes before and after dip-coating reflective layer. PCE value of IPVFs for comparison was presented as the mean ± standard deviation of three measured IPVFs at least. The PCE variation is defined as the standard deviation of PCE divided by its average value.

Supporting Information

Supporting Information is available from the Wiley Online Library or from the author.

Acknowledgements

Z.Z., Z.L., and Y.G. contributed equally to this work. This work was supported by MOST (2022YFA1203001, 2022YFA1203002), NSFC (T2321003, 22335003), STCSM (21511104900 and 20JC1414902), Natural Science Foundation of Jiangsu Province (BK20200071), and China Postdoctoral Science Foundation (2021M690659).

Conflict of Interest

The authors declare no conflict of interest.

Data Availability Statement

The data that support the findings of this study are available from the corresponding author upon reasonable request.

Keywords

carbon nanotubes, dye-sensitized solar cells, fibers, porous structures, reflective layer

Received: June 14, 2023
Revised: August 19, 2023
Published online: September 13, 2023

[1] X. Shi, Y. Zuo, P. Zhai, J. Shen, Y. Yang, Z. Gao, M. Liao, J. Wu, J. Wang, X. Xu, Q. Tong, B. Zhang, B. Wang, X. Sun, L. Zhang, Q. Pei, D. Jin, P. Chen, H. Peng, *Nature* **2021**, *591*, 240.
[2] G. Chen, X. Xiao, X. Zhao, T. Tat, M. Bick, J. Chen, *Chem. Rev.* **2022**, *122*, 3259.
[3] M. Chao, P. Di, Y. Yuan, Y. Xu, L. Zhang, P. Wan, *Nano Energy* **2023**, *108*, 108201.
[4] A. Libanori, G. Chen, X. Zhao, Y. Zhou, J. Chen, *Nat. Electron.* **2022**, *5*, 142.
[5] Y. Zhang, X. Xia, K. Ma, G. Xia, M. Wu, Y. H. Cheung, H. Yu, B. Zou, X. Zhang, O. K. Farha, J. H. Xin, *Adv. Funct. Mater.* **2023**, *33*, 2301607.
[6] C. Chen, J. Feng, J. Li, Y. Guo, X. Shi, H. Peng, *Chem. Rev.* **2023**, *123*, 613.
[7] Y. Liu, X. Zhou, H. Yan, Z. Zhu, X. Shi, Y. Peng, L. Chen, P. Chen, H. Peng, *Adv. Funct. Mater.* **2022**, *32*, 2201510.
[8] Z. Zhang, X. Chen, P. Chen, G. Guan, L. Qiu, H. Lin, Z. Yang, W. Bai, Y. Luo, H. Peng, *Adv. Mater.* **2014**, *26*, 466.
[9] L. Qiu, J. Deng, X. Lu, Z. Yang, H. Peng, *Angew. Chem., Int. Ed. Engl.* **2014**, *53*, 10425.
[10] R. E. A. Ardhi, M. X. Tran, M. Wang, G. Liu, J. K. Lee, *J. Mater. Chem. A* **2020**, *8*, 2549.
[11] X. Kang, Z. Zhu, T. Zhao, W. Zhai, J. Xu, Z. Lin, K. Zeng, B. Wang, X. Sun, P. Chen, H. Peng, *Adv. Funct. Mater.* **2022**, *32*, 2207763.
[12] W. Zhai, Z. Zhu, X. Sun, H. Peng, *Adv. Fiber Mater.* **2022**, *4*, 1293.
[13] X. Fu, H. Sun, S. Xie, J. Zhang, Z. Pan, M. Liao, L. Xu, Z. Li, B. Wang, X. Sun, H. Peng, *J. Mater. Chem. A* **2018**, *6*, 45.
[14] J. Zhang, Z. Wang, X. Li, J. Yang, C. Song, Y. Li, J. Cheng, Q. Guan, B. Wang, *ACS Appl. Energy Mater.* **2019**, *2*, 2870.
[15] Z. Zhou, S. Sigdel, J. Gong, B. Vaagensmith, H. Elbohy, H. Yang, S. Krishnan, X. F. Wu, Q. Qiao, *Nano Energy* **2016**, *22*, 558.
[16] G. Liu, M. Wang, H. Wang, R. E. A. Ardhi, H. Yu, D. Zou, J. K. Lee, *Nano Energy* **2018**, *49*, 95.
[17] Z. Zhu, Z. Lin, W. Zhai, X. Kang, J. Song, C. Lu, H. Jiang, P. Chen, X. Sun, B. Wang, Z. Wang, H. Peng, *Adv. Mater.* **2023**, 2304876, https://doi.org/10.1002/adma.202306504.
[18] L. Qiu, S. He, J. Yang, J. Deng, H. Peng, *Small* **2016**, *12*, 2419.
[19] D. Lv, Q. Jiang, Y. Shang, D. Liu, *npj Flexible Electron.* **2022**, *6*, 38.
[20] A. Rafique, I. Ferreira, G. Abbas, A. C. Baptista, *Nanomicro Lett.* **2023**, *15*, 40.
[21] X. Meng, C. Yu, X. Song, J. Iocozzia, J. Hong, M. Rager, H. Jin, S. Wang, L. Huang, J. Qiu, Z. Lin, *Angew. Chem., Int. Ed.* **2018**, *57*, 4682.
[22] L. Yao, Q. Wu, P. Zhang, J. Zhang, D. Wang, Y. Li, X. Ren, H. Mi, L. Deng, Z. Zheng, *Adv. Mater.* **2018**, *30*, 1706054.
[23] X. Meng, C. Yu, X. Zhang, L. Huang, M. Rager, J. Hong, J. Qiu, Z. Lin, *Nano Energy* **2018**, *54*, 138.
[24] H. Zhang, W. Zhao, M. Zou, Y. Wang, Y. Chen, L. Xu, H. Wu, A. Cao, *Adv. Energy Mater.* **2018**, *8*, 1800013.
[25] J. Peoples, X. Li, Y. Lv, J. Qiu, Z. Huang, X. Ruan, *Int. J. Heat Mass Transfer* **2019**, *131*, 487.
[26] J. L. Saunderson, *J. Opt. Soc. Am.* **1942**, *32*, 727.
[27] B. Orel, M. K. Gunde, A. Krainer, *Sol. Energy* **1993**, *50*, 477.
[28] A. K. Roy Choudhury, in *Principles of Colour and Appearance Measurement* (Ed: A. K. Roy Choudhury), Woodhead Publishing, Oxford **2015**.
[29] J. Zhu, Z. An, A. Zhang, Y. Du, X. Zhou, Y. Geng, G. Chen, *iScience* **2022**, *25*, 104126.
[30] B. Xiang, R. Zhang, Y. Luo, S. Zhang, L. Xu, H. Min, S. Tang, X. Meng, *Nano Energy* **2021**, *81*, 105600.
[31] J. Mandal, Y. Fu, A. C. Overvig, M. Jia, K. Sun, N. N. Shi, H. Zhou, X. Xiao, N. Yu, Y. Yang, *Science* **2018**, *362*, 315.
[32] V. Vand, *Nature* **1945**, *155*, 364.
[33] H. C. Brinkman, *J. Chem. Phys.* **1952**, *20*, 571.
[34] W. Duangthongsuk, S. Wongwises, *Exp. Therm. Fluid Sci.* **2009**, *33*, 706.
[35] H. C. Hulst, H. C. van de Hulst, *Light Scattering by Small Particles*, Courier Corporation, New York, **1981**.
[36] P. Chýlek, J. Zhan, *J. Opt. Soc. Am. A* **1989**, *6*, 1846.
[37] T. Wang, Y. Wu, L. Shi, X. Hu, M. Chen, L. Wu, *Nat. Commun.* **2021**, *12*, 365.
[38] J. Song, J. Qin, J. Qu, Z. Song, W. Zhang, X. Xue, Y. Shi, T. Zhang, W. Ji, R. Zhang, H. Zhang, Z. Zhang, X. Wu, *Sol. Energy Mater. Sol. Cells* **2014**, *130*, 42.
[39] S. Zeng, S. Pian, M. Su, Z. Wang, M. Wu, X. Liu, M. Chen, Y. Xiang, J. Wu, M. Zhang, Q. Cen, Y. Tang, X. Zhou, Z. Huang, R. Wang, A. Tunuhe, X. Sun, Z. Xia, M. Tian, M. Chen, X. Ma, L. Yang, J. Zhou, H. Zhou, Q. Yang, X. Li, Y. Ma, G. Tao, *Science* **2021**, *373*, 692.
[40] S. Hrapovic, Y. Liu, K. B. Male, J. H. T. Luong, *Anal. Chem.* **2004**, *76*, 1083.